Thin Solid Films 520 (2012) 2938–2942

Contents lists available at SciVerse ScienceDirect

Thin Solid Films

journal homepage: www.elsevier.com/locate/tsf

Pulsed-laser deposition of heteroepitaxial corundum-type ZITO: *cor*-$In_{2-2x}Zn_xSn_xO_3$

Cathleen A. Hoel [a], D. Bruce Buchholz [b], Robert P.H. Chang [b], Kenneth R. Poeppelmeier [a,*]

[a] Department of Chemistry, Northwestern University, 2145 Sheridan Road, Evanston, IL 60208, USA
[b] Department of Materials Science and Engineering, 2220 Campus Drive, Evanston, IL 60208, USA

ARTICLE INFO

Article history:
Received 13 February 2011
Received in revised form 29 September 2011
Accepted 10 October 2011
Available online 15 October 2011

Keywords:
Transparent conducting oxide
Pulsed-laser deposition
Epitaxial
Zinc indium tin oxide
Lattice matched
Corundum

ABSTRACT

Thin films of corundum-type $In_{2-2x}Zn_xSn_xO_3$ (*cor*-ZITO) were grown on lattice-matched substrates using pulsed laser deposition. The (001) of the corundum-type film grew heteroepitaxial to the (001) of a $LiNbO_3$ substrate with large grains along the in-plane and out-of-plane orientation characterized by glancing incidence X-ray diffraction and four-circle Φ-scans. A film with 34% In (metals basis) exhibited a wide optical gap of 3.9 eV and a modest conductivity of 134 S/cm, which suggests *cor*-ZITO is a potential low-cost transparent conducting oxide.

1. Introduction

Transparent conducting oxides (TCOs) are materials necessary for opto-electronic devices owing to their simultaneous visible transparency and electrical conductivity [1,2]. The most popular TCO for high-performance electronic devices, such as flat-panel displays, is tin-doped indium oxide (ITO). Indium metal, however, is costly and becoming scarce owing to increased demand, which has encouraged the development of alternative TCOs. Zn and Sn cosubstituted In_2O_3 ($In_{2-2x}Zn_xSn_xO_3$, ZITO) has the potential to replace ITO owing to its competitive conductivity and transparency at lower indium content [3–5]. The development of ZITO for the application as a TCO has focused on the stable bixbyite polymorph, *bix*-ZITO, which can maintain a single-phase crystalline structure with up to 40% Zn/Sn cosubstitution ($x \leq 0.4$) in the bulk form.

Recently, the corundum-type polymorph, *cor*-ZITO, has been reported to exhibit an extended Zn/Sn cosubstitution solubility of 70% ($x \leq 0.7$) when synthesized by high-pressure solid state reaction [6]. *cor*-ZITO is metastable with *bix*-ZITO [7,8], but once formed has a demonstrated thermal stability up to 850 °C in the bulk form [8] making it suitable for use in devices. After a new TCO has been synthesized in the bulk form, thin film growth methods must be developed for device implementation. Thin films of *cor*-In_2O_3 have been grown by metal organic chemical vapor deposition [9–11] and *cor*-ITO films of these nominally bixbyite materials have been deposited using sol–gel spin coating [12–14]. This poses the possibility that *cor*-ZITO, with its extended Zn/Sn cosubstitution solubility, could also be deposited in thin-film form. The formation of specific thin film phases can be facilitated by the use of substrates latticed-matched to the desired thin film phase. Son et al. [15] reported the deposition of a heteroepitaxial corundum structure type $ZnSnO_3$ film (*cor*-$ZnSnO_3$). The single-phase corundum-type structure for $ZnSnO_3$ was favored over a Zn_2SnO_4/SnO_2 mixture through use of a lattice matching $SrRuO_3(111)/SrTiO_3(111)$ substrate. In this work, a $LiNbO_3(001)$ substrate (*R3c*, $a = 5.148$ Å, 13.863 Å) is used to induce formation of the targeted *cor*-$In_{0.6}Zn_{0.7}Sn_{0.7}O_3$ phase (*R-3c*, $a = 5.341$ Å, $c = 14.275$ Å) by way of lattice matching. The mismatch between the {001} $LiNbO_3$ and {001} *cor*-$In_{0.6}Zn_{0.7}Sn_{0.7}O_3$ planes is calculated as 3.6%. This work also investigates films grown on a non-lattice-matched substrate, $Al_2O_3(001)$ (i.e., sapphire; *R-3c*, $a = 4.785$ Å, $c = 12.991$ Å), and an amorphous substrate, fused silica, for comparison.

2. Experimental details

A two-inch diameter, 0.5 mm thick, *z*-cut, double-sided polished $LiNbO_3$ wafer and α-Al_2O_3 wafer were purchased from MDI Supplies and cut into 1×1 cm^2 pieces. The substrates were cleaned by sonication in acetone, rinsed with ethanol and blown dry with an air stream. Thin-film ZITO specimens were grown by pulsed-laser deposition (PLD) from a dense hot-pressed ceramic target described below. PLD was accomplished with a 248 nm KrF excimer laser with a 25 ns pulse duration and operated at 2 Hz. The 200 mJ/pulse beam was focused onto a 1 mm × 2 mm spot size. The target was rotated at 5-rpm about its axis to prevent localized heating. The target-substrate separation was fixed at 8 cm. The films were grown in an

* Corresponding author at: 2145 Sheridan Road, Evanston, IL 60208, USA. Tel.: +1 847 491 3505; fax: +1 847 491 7713.
E-mail addresses: c-hoel@u.northwestern.edu (C.A. Hoel), d-buchholz@northwestern.edu (D.B. Buchholz), r-chang@northwestern.edu (R.P.H. Chang), krp@northwestern.edu (K.R. Poeppelmeier).

0040-6090/$ – see front matter © 2011 Elsevier B.V. All rights reserved.
doi:10.1016/j.tsf.2011.10.012

O_2 ambient at pressures of $pO_2 = 0.67$, 1.33 and 6.67 Pa (or 5, 10 and 50 mTorr) as noted in the text. The films were grown at a deposition temperature of 500 °C by adhering the substrates to a resistively-heated substrate holder with silver paint. The powder used to make the target was prepared by mixing the molar ratios 0.3 $InO_{1.5}$:0.35 ZnO:0.35 SnO_2. According to the subsolidus phase diagram this composition yields a mixture of bixbyite-ZITO, In-substituted Zn_2SnO_4 and SnO_2 when reacted at 1275 °C [16]. The powder was ground with a mortar and pestle, pressed into pellets and fired at 1000 °C for 24 h surrounded by sacrificial powder of the same composition. The annealed pellets were reground and pressed into a pellet 1 in. in diameter and 0.25 in. thick, which was sintered at 1250 °C for 24 h surrounded by sacrificial powder to minimize ZnO vaporization.

A Rigaku ATX-G X-ray diffraction spectrometer was used to identify the phases present by glancing incidence X-ray diffraction (GI-XRD). The X-ray beam was filtered through two Ge(111) monochromators to select the Cu Kα1 wavelength. The films were scanned over the range $2\theta = 10$–95° at a scan speed of 4°/min. The out-of-plane and in-plane crystallinity were determined by the four-circle method also using Cu Kα1 radiation on a Rigaku RU-200PL diffractometer. The $LiNbO_3$(001) substrate and film were positioned at $\chi = 32.75°$ and 32.86°, respectively, and Φ-scans performed on the (012) reflections of the substrate and film from 0 to 360°. The $LiNbO_3$ substrate was scanned with a 0.1° step size and 1.0 s dwell time and the film was scanned with a 0.1° step size and 5.0 s dwell time. Rocking curves of the film (006) and (012) diffraction peaks were collected with a 0.05° step size and 10 s dwell time as a measure of the in-plane and out-of-plane crystallinity respectively.

The sheet resistance, areal carrier concentration and mobility of the films were measured with a Bio-Rad Microscience LTD HL5500 Hall measurement system (Hertfordshire, UK) using the van der Pauw geometry. The sheet resistance of each film was measured at three different voltages (5, 10 and 20 mV) and with the probe contacts on two different sites for a total of six conductivity measurements per film. The values reported are the average and standard deviation of the six measurements. One film was annealed under forming gas (5% H_2/bal. N_2) for 1 h at 400 °C, after which the sheet resistance was remeasured. The conductivity, σ, was determined using $\sigma = (\rho_s t)^{-1}$ where ρ_s is the sheet resistance and t is the film thickness.

The UV–vis absorption spectra of the films were measured in transmission mode with a PerkinElmer Integrating Sphere with a 150 mm UV/vis/NIR (InGaAs) Module (PE Lambda 1050). The absorption was calculated using the formula $A = -\ln(T)$, where T is the fraction of transmittance. The absorption coefficient, α, was calculated by dividing the absorption by the film thickness. For crystalline films, the optical band gap was determined by plotting $(\alpha h\nu)^2$ versus $(h\nu)$ and extrapolating the linear portion of the curve to the x-intercept. For amorphous films a plot of $(\alpha h\nu)^{1/2}$ versus $(h\nu)$ was used, again extrapolating the linear portion of the curve to the x-intercept. The film thicknesses were calculated based on the number of laser pulses used to deposit the films. The thicknesses of films grown under similar conditions, and measured by step-edge profilometry and/or ellipsometry, were used to calibrate the per-pulse deposition rate.

The composition of the films was measured using a variable pressure Hitachi S3400N-II scanning electron microscope equipped with an Oxford energy dispersive spectroscopy (EDS) system. Area sampling and point sampling yielded comparable composition values. For point sampling, an average of at least five points was used. The standard deviation of the EDS measurements was about 10%.

3. Results

3.1. Structural characterization

Three deposition conditions were used to grow a total of six films. For each deposition, the substrates were heated to 500 °C. A single film was grown at $pO_2 = 1.33$ Pa on a $LiNbO_3$ substrate (FilmLN10). The film thickness was 360 nm and the average composition $In_{0.68}Zn_{0.59}Sn_{0.73}O_{3-\delta}$. Two films were grown at $pO_2 = 6.67$ Pa; one on a $LiNbO_3$ substrate (FilmLN50) and one on an Al_2O_3 substrate (FilmAL50). The $LiNbO_3$ and Al_2O_3 substrates were placed side-by-side on the substrate holder such that FilmLN50 and FilmAL50 could be grown under identical conditions during a single deposition. The film thickness for FilmLN50 and FilmAL50 was 600 nm and the average composition $In_{0.66}Zn_{0.58}Sn_{0.76}O_{3-\delta}$. Three films were grown at $pO_2 = 0.67$ Pa: one on a $LiNbO_3$ substrate (FilmLN05), one on an Al_2O_3 substrate (FilmAL05), and one on a fused silica substrate (FilmFS05). The three substrates were placed adjacent to each other on the substrate holder such that the three films could be grown under identical deposition conditions during a single deposition. The film thickness for FilmLN05, FilmAL05 and FilmFS05 was 600 nm and the average composition $In_{0.72}Zn_{0.50}Sn_{0.78}O_{3-\delta}$. The deposition conditions, identified phases, as well as the electrical and optical properties of each film, are summarized in Table 1.

GI-XRD revealed heteroepitaxial growth of *cor*-ZITO(001) on the $LiNbO_3$(001) substrates under all three growth conditions. FilmLN10 and FilmLN50 each exhibited a strong diffraction peak at $2\theta = 37.44°$ and a weak peak at $2\theta = 79.91°$, which can be assigned to the *cor*-ZITO (006) and (0,0,12) reflections, respectively. The (006) and (0,0,12) reflections of the $LiNbO_3$ substrate were at the expected 2θ positions ensuring proper instrument alignment. The GI-XRD pattern of FilmLN10 is shown in Fig. 1. Based on the 2θ positions of the peaks, the films grown on $LiNbO_3$(001) at 10 and 50 mTorr have an estimated lattice constant of $c = 14.402$ Å. FilmLN05, which was grown on $LiNbO_3$ at 0.67 Pa pO_2, exhibited the (006) reflection at $2\theta = 37.25°$ and the (0,0,12) at 79.40° giving a larger lattice parameter of $c = 14.475$ Å. The smaller diffraction angle (larger lattice parameter) for FilmLN05 than those observed for FilmLN10 and FilmLN50 (Fig. 2) suggests less Zn and Sn substitution [3,16]. Harvey et al. [4] demonstrated that lower pO_2 during PLD depositions can lead to less Zn in the film owing to its relatively high volatility. This is also consistent with the lower percentage of Zn measured in FilmLN05 ($In_{0.72}Zn_{0.50}Sn_{0.78}O_{3-\delta}$) compared to FilmLN10 ($In_{0.68}Zn_{0.59}Sn_{0.73}O_{3-\delta}$) and FilmLN50 ($In_{0.66}Zn_{0.58}Sn_{0.76}O_{3-\delta}$).

FilmAL50 and FilmAL05, which were deposited on Al_2O_3(001) substrates, each exhibited very weak diffraction peaks that appear at 2θ ~37.4° where the (006) reflection of *cor*-ZITO would be observed. The intensity, however, was very low as demonstrated in Fig. 3; therefore, FilmAL50 and FilmAL05 were considered to be predominately amorphous. The GI-XRD of FilmFS05 revealed peaks that were broad and occurred at the same 2θ positions as *bix*-In_2O_3, but with different intensities, likely from preferred orientation (Fig. 4). The GI-XRD pattern also showed a high background signal, which is typically associated with secondary amorphous phases.

The in-plane orientation of FilmLN10 ($pO_2 = 1.33$ Pa, $LiNbO_3$ substrate) was examined by performing Φ-scans. A Φ-scan of the (012) for the $LiNbO_3$ substrate ($\chi = 32.75°$) revealed the expected three-fold symmetry, as shown in Fig. 5. A Φ-scan of the (012) of FilmLN10, observed at $2\theta = 22.956°$ and $\chi = 32.86°$, revealed six-fold symmetry, also shown in Fig. 5. The six-fold symmetry was attributed to twinning, which was also observed by Son et al. [15] for the epitaxial growth of *cor*-$ZnSnO_3$ films. The relative positions of the in-plane peaks indicate epitaxial growth of *cor*-ZITO(001) on $LiNbO_3$(001) such that the *c*-axis of *cor*-ZITO is parallel to the *c*-axis of the $LiNbO_3$ substrate. A rocking curve on the FilmLN10 (006) diffraction peak, plotted in Fig. 6, showed a full-width at half maximum (FWHM) of 0.36° indicating large crystalline grains along the out-of-plane orientation. A rocking curve of the FilmLN10 (012), shown in Fig. 6, had a FWHM of 1.26° indicating moderately large grains along the in-plane orientation. The 2θ positions of the (006) and (012) reflections were used to estimate the lattice parameters to be $a = 5.370$ Å and $c = 14.404$ Å for FilmLN10. The lattice parameters of

Table 1
Summary of film deposition conditions, observed phases and electrical and optical properties.

	Substrate	pO_2 (Pa)	Phases	E_g (eV)	σ (S/cm.)	μ (cm^2/Vs)	n ($\times 10^{19}$ cm^{-3})	T (%)
FilmLN05	$LiNbO_3$	0.67	*cor*-ZITO	3.95	134	20.7(1.5)	4.08	72.6
FilmLN10	$LiNbO_3$	1.33	*cor*-ZITO	3.85	101	31.0(1.3)	2.04	67.9
FilmLN50	$LiNbO_3$	6.67	*cor*-ZITO	3.83	24.4	20.2(4)	0.753	69.1
FilmAL05	Al_2O_3	0.67	Amorphous	3.02	93.8	18.8(9)	3.13	79.9
FilmAL50	Al_2O_3	6.67	Amorphous	3.15	9.63	11.2(7)	0.547	80.4
FilmFS05	Fused SiO_2	0.67	In_2O_3, amorphous	3.00	<0.833	–	–	73.8
FilmLN10 reduced	$LiNbO_3$	1.33	*cor*-ZITO	3.94	186	31.0	2.04	65.6

the bulk solid solution are reported by Hoel, et al. [6]. Both the *a* and *c*-axes are larger for FilmLN10 than bulk *cor*-ZITO at $x=0.7$ ($a_{bulk}=5.341$, $c_{bulk}=14.275$ Å). The larger lattice of the film may be due to a lower Zn and Sn substitution, closer to $x\approx 0.5$ ($a_{bulk}=5.383$, $c_{bulk}=14.360$ Å). The *c*/*a* ratio of FilmLN10 (2.682) is slightly larger than the *c*/*a* ratio of bulk *cor*-ZITO for $x=0.5$, (2.668). The residual mismatch between the substrate and film lattice parameters may have contributed to a contracted in-plane lattice constant, which would lead to an expanded out-of-plane lattice constant and account for the small deviation of the film lattice parameters from the bulk.

3.2. Electrical properties

The electrical behavior can be compared for films grown on the same substrate with different pO_2 or for films grown under the same pO_2 on different substrates (Table 1). FilmLN05, which was grown on the $LiNbO_3$ substrate at $pO_2=0.67$ Pa, had the highest σ at 134 S/cm. As the pO_2 was increased for FilmLN10 and FilmLN50, σ decreased to 101 and 24 S/cm, respectively. Likewise, FilmAL05 had a conductivity of 93 S/cm and was grown under $pO_2=0.67$ Pa while FilmAL50 had a lower σ of 9.6 S/cm and was grown under a higher pO_2 of 6.67 Pa. The observed trend of higher conductivity with lower pO_2 during depositions is typical for n-type TCOs. FilmLN10 was annealed under forming gas (5% H_2, 95% N_2) at 400 °C for 1 h, which increased the conductivity from 101 to 186 S/cm. Of the three films grown under the low $pO_2=5$ mTorr, FilmLN05 had the highest conductivity of 134 S/cm followed by FilmAL05 with $\sigma=93$ S/cm. FilmFS05, on the other hand, had a conductivity that was too low to accurately measure with the Hall apparatus despite the low pO_2 present during the deposition. The conductivity of the epitaxial *cor*-ZITO films was not as high as those typically observed for *bix*-ITO or *bix*-ZITO ($\sigma>1000$ S/cm), but *cor*-ZITO is competitive with ZnO–SnO_2 films ($\sigma\approx 100$ S/cm) [5]. Further studies of the doping mechanism and deposition effects, or insertion of an Ag layer [17], could lead to designing films with higher conductivities.

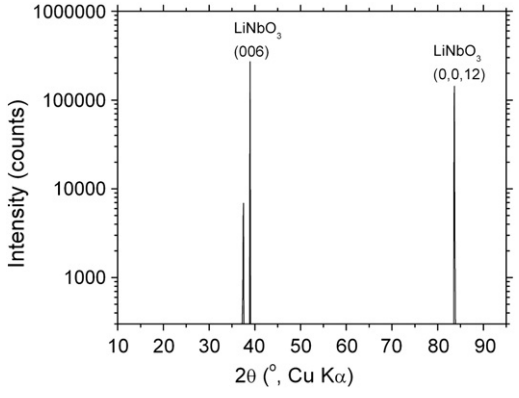

Fig. 1. GIXRD θ–2θ scan of FilmLN10. The $LiNbO_3$ (006) and (0,0,12) peaks are labeled. The *cor*-ZITO (006) peak is located at $2\theta=37.44°$. The film (0,0,12) reflection, too weak to see at this scale, is located at $2\theta=79.91°$.

3.3. Optical properties

The average optical transmittance value from 400–800 nm for the collection of films ranges from 66% to 80% (Fig. 7). The optical band gap of each film and the average transmittance, T, over the 400–800 nm band are listed in Table 1. The optical band gaps of the epitaxial *cor*-ZITO films (FilmLN05, FilmLN10 and FilmLN50) were over 3.8 eV and increase with increased carrier concentration, consistent with the Burstein–Moss effect [18]. The band gap of *cor*-In_2O_3 has been reported as 3.16 eV [11]. The wider band gaps observed for *cor*-ZITO compared to *cor*-In_2O_3 may be attributed to the substitution of Zn and Sn. Band gap widening with increasing Zn and Sn was observed prior for bulk *bix*-ZITO [3]. The amorphous films (FilmAL05, FilmAL50, FilmFS05) had optical band gaps near 3.1 eV, which are wider than previously reported amorphous ZITO films grown with compositions near $In_{1.4}Zn_{0.3}Sn_{0.3}O_3$ [19].

4. Discussion

4.1. Effect of pO_2

Films that were deposited with lower pO_2 exhibited higher σ owing to increased carrier concentrations, which is typical for n-type TCOs. Likewise, a reducing anneal under forming gas yielded a conductivity increase from 101 S/cm ($\mu=31.0$ cm^2/Vs, $n=2.04\times10^{19}$ cm^{-3}) to 186 S/cm ($\mu=38.1$ cm^2/Vs, $n=3.05\times10^{19}$ cm^{-3}). Electron generation is often attributed to oxygen vacancies, but other donor sources, such as off-stoichiometric Sn:Zn ratios, have been suggested as significant electron donors for In_2O_3-based TCOs [3,4,20–22]. The mechanism for electron generation is not known for *cor*-ZITO or *cor*-In_2O_3.

4.2. Effect of substrate

The results of the GI-XRD and Φ-scans demonstrated that the $LiNbO_3$(001) substrate directed the formation of epitaxial *cor*-ZITO(001) thin films by way of lattice matching. Although

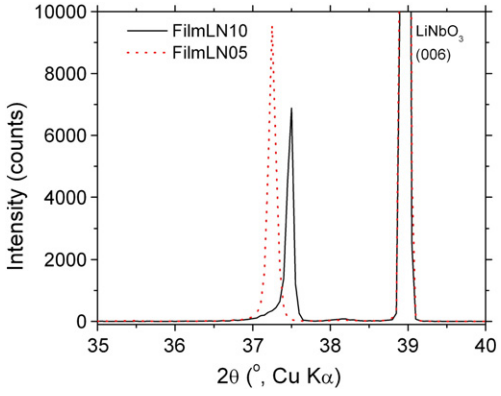

Fig. 2. The GIXRD θ–2θ scans of FilmLN10 and FilmLN05. The (006) reflection of FilmLN05 appears at a lower angle than the (006) of FilmLN10.

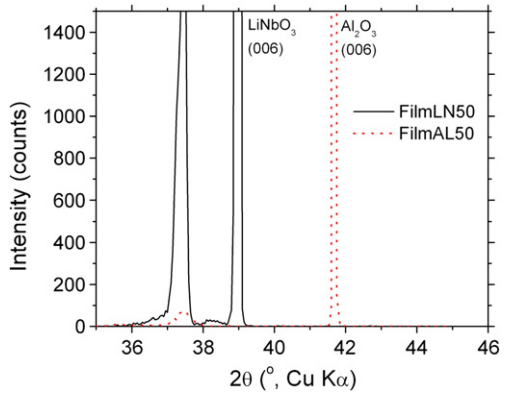

Fig. 3. The GIXRD θ–2θ scans of FilmLN50 and FilmAL50. The strongest film peak observed for FilmAL50 is at 2θ ~37.4° and has very low intensity.

$Al_2O_3(001)$ is isostructural with *cor*-ZITO, the >10% mismatch was too large to stabilize *cor*-ZITO(001). Amorphous films were observed with conductivities that were modestly lower than those of epitaxial *cor*-ZITO. The electron mobilities of the crystalline *cor*-ZITO films and the amorphous films are all within 10–30 cm^2/Vs. The carrier concentration of FilmLN05 at $n = 4.08 \times 10^{19}\ cm^{-3}$ is slightly higher than FilmAL05 with $n = 3.13 \times 10^{19}\ cm^{-3}$. It is not well understood why comparable electrical properties are observed for crystalline and amorphous TCOs and elucidating these structure–property relationships has become a growing research interest [19,23]. The film with the lowest σ, FilmFS05, was a mixture of poorly crystalline *bix*-In_2O_3 and amorphous phases, which likely inhibited electron transport. Even though FilmLN05 and FilmFS05 have the same composition and were prepared under the same deposition conditions, FilmLN05 is a moderate conductor while FilmFS05 is a very poor conductor.

5. Conclusion

Heteroepitaxial thin films were grown of the metastable *cor*-ZITO polymorph induced by a lattice-matched substrate, $LiNbO_3$. Lower pO_2 during depositions and reducing anneals led to higher conductivities. The pO_2 during deposition also affected the relative concentration of the metal cations, such that less Zn was present in the *cor*-ZITO phase with the lowest pO_2. The use of the $LiNbO_3$ substrate yielded highly crystalline and epitaxial thin films with conductivities one order of magnitude lower than typical *bix*-ITO and *bix*-ZITO conductivity. When a fused silica substrate was used, a mixture of phases was observed and σ was too low to measure. This study exemplifies the importance of the crystalline structure to obtain a high doping

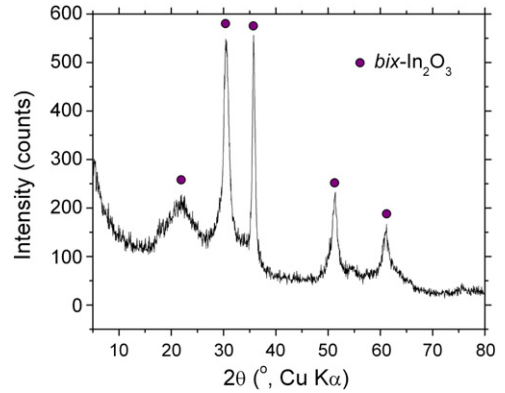

Fig. 4. GIXRD of FilmFS05. Peaks corresponding to *bix*-In_2O_3 reflections are marked with a purple circle.

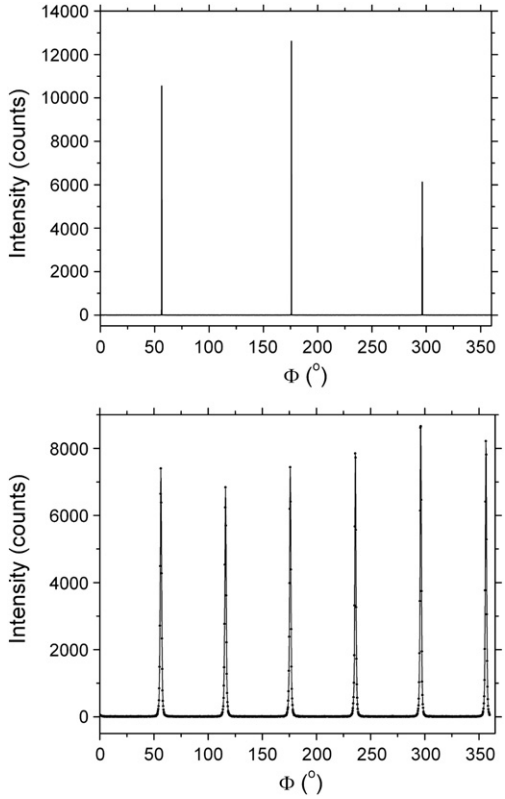

Fig. 5. Φ-scans of the (012) for the $LiNbO_3$ substrate and FilmLN10 pictured on the top and bottom, respectively.

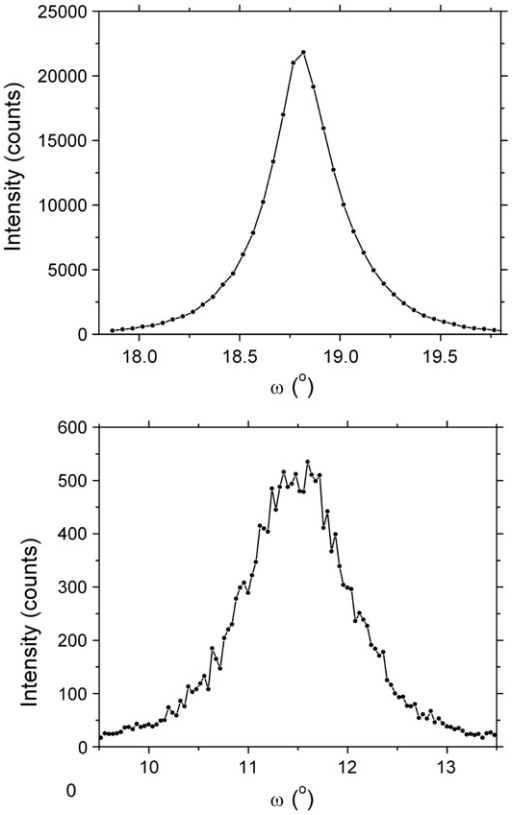

Fig. 6. Rocking curves of the FilmLN10 (006) and (012) peaks pictured on the top and bottom, respectively.

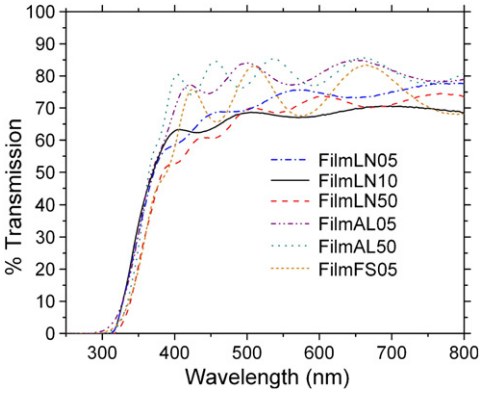

Fig. 7. Transmittance spectra of thin films plotted versus wavelength.

level and electron mobility in a thin film. This work also demonstrates using knowledge of the crystal structure of a previously synthesized bulk material to target the phase as a thin film, in this case with a lattice-matched substrate. Further studies are warranted because they could lead to optimizing *cor*-ZITO such that it is competitive with ITO, while using a low indium content.

Acknowledgments

C.A.H. was funded through support of the Materials Research Science and Engineering Center at Northwestern University supported by the National Science Foundation under NSF Award Number DMR-050513. The amorphous ZITO work is based upon work supported as part of ANSER, an Energy Frontier Research Center funded by the U.S. Department of Energy, Office of Science, Office of Basic Energy Sciences under Award Number DE-SC0001059. The authors gratefully acknowledge additional support for the crystalline ZITO work from the Department of Energy Basic Energy Sciences under Award no. DE-FG02-08ER46536. This work made use of the J.B. Cohen X-ray Facility supported by the MRSEC program of the National Science Foundation (DMR-0520513) at the Materials Research Center of Northwestern University. This work was supported by the Northwestern University Keck Biophysics Facility and a Cancer Center Support Grant (NCI CA060553) for the optical measurements. This work made use of the Electron Probe Instrumentation Center (EPIC) and the Optical Microscopy and Metallography Facility, which are supported by the NU-MRSEC program. C.A.H. thanks A. Raw and S. Pease-Dodson for the EDS measurements and J. Carsello and B. Stevens for help with the four-circle XRD scans and discussions. C.A.H. and K.R.P. thank T.O. Mason and D.E. Proffit for helpful discussions.

References

[1] P.P. Edwards, A. Porch, M.O. Jones, D.V. Morgan, R.M. Perks, Dalton Trans. 19 (2004) 2995.
[2] E. Fortunato, D. Ginley, H. Hosono, D.C. Paine, MRS Bull. 32 (3) (2007) 242.
[3] G.B. Palmer, K.R. Poeppelmeier, T.O. Mason, Chem. Mater. 9 (1997) 3121.
[4] S.P. Harvey, T.O. Mason, D.B. Buchholz, R.P.H. Chang, C. Korber, A. Klein, J. Am. Ceram. Soc. 91 (2) (2008) 467.
[5] C.A. Hoel, T.O. Mason, J.-F. Gaillard, K.R. Poeppelmeier, Chem. Mater. 22 (2010) 3569.
[6] C.A. Hoel, J.M.G. Amores, M.A. Alario-Franco, E. Moran, J.-F. Gaillard, K.R. Poeppelmeier, J. Am. Chem. Soc. 132 (2010) 16479.
[7] A. Gurlo, P. Kroll, R. Riedel, Chem. Eur. J. 14 (2008) 3306.
[8] C.A. Hoel, Ph.D. Thesis, Department of Chemistry, Northwestern University, Evanston, 2010.
[9] C.Y. Wang, V. Cimalla, H. Romanus, T. Kups, G. Ecke, T. Stauden, M. Ali, V. Lebedev, J. Pezoldt, O. Ambacher, Appl. Phys. Lett. 89 (2006) 011904.
[10] C.Y. Wang, V. Cimalla, H. Romanus, T. Kups, M. Niebelschutz, O. Ambacher, Thin Solid Films 515 (2007) 6611.
[11] P.D.C. King, T.D. Veal, F. Fuchs, C.Y. Wang, D.J. Payne, A. Bourlange, H. Zhang, G.R. Bell, V. Cimalla, O. Ambacher, R.G. Egdell, F. Bechstedt, C.F. McConville, Phys. Rev. B 79 (2009) 205211.
[12] C.T. Prewitt, R.D. Shannon, D.B. Rodgers, A.W. Sleight, Inorg. Chem. 8 (9) (1969) 1985.
[13] D. Yu, W. Yu, D. Wang, Y. Qian, Thin Solid Films 419 (2002) 166.
[14] K.-H. Seo, J.-H. Lee, J.-J. Kim, M.I. Bertoni, B.J. Ingram, T.O. Mason, J. Am. Ceram. Soc. 89 (2006) 3431.
[15] J.Y. Son, G. Lee, M.-H. Jo, H. Kim, H.M. Jang, Y.-H. Shin, J. Am. Chem. Soc. 131 (2009) 8386.
[16] S.P. Harvey, K.R. Poeppelmeier, T.O. Mason, J. Am. Ceram. Soc. 91 (11) (2008) 3683.
[17] Y.-S. Park, H.-K. Kim, S.-W. Kim, J. Electrochem. Soc. 157 (2010) J301.
[18] E. Burstein, Phys. Rev. 93 (1954) 632.
[19] D.B. Buchholz, J. Liu, T.J. Marks, M. Zhang, R.P.H. Chang, Appl. Mater. Interfac. 1 (2009) 2147.
[20] A. Ambrosini, S. Malo, K.R. Poeppelmeier, M.A. Lane, C.R. Kannewurf, T.O. Mason, Chem. Mater. 14 (2002) 58.
[21] A. Ambrosini, G.B. Palmer, A. Maignan, K.R. Poeppelmeier, M.A. Lane, P. Brazis, C.R. Kannewurf, T. Hogan, T.O. Mason, Chem. Mater. 14 (2002) 52.
[22] T. Moriga, D.D. Edwards, T.O. Mason, G.B. Palmer, K.R. Poeppelmeier, J.L. Schindler, C.R. Kannewurf, I. Nakabayashi, J. Am. Ceram. Soc. 81 (5) (1998) 1310.
[23] T. Kamiya, H. Hosono, NPG Asia Mater. 2 (2010) 15.